# Chapter 15
# Astronomy and Cancer Research: X-Rays and Nanotechnology from Black Holes to Cancer Therapy

**Anil K. Pradhan and Sultana N. Nahar**

**Abstract** It seems highly unlikely that any connection is to be found between astronomy and medicine. But then it also appears to be obvious: X-rays. However, that is quite superficial because the nature of X-rays in the two disciplines is quite different. Nevertheless, we describe recent research on exactly that kind of link. Furthermore, the linkage lies in atomic physics, and via spectroscopy which is a vital tool in astronomy and may also be equally valuable in biomedical research. This review begins with the physics of black hole environments as viewed through X-ray spectroscopy. It is then shown that similar physics can be applied to spectroscopic imaging and therapeutics using heavy-element (high-$Z$) moieties designed to target cancerous tumors. X-ray irradiation of high-$Z$ nanomaterials as radiosensitizing agents should be extremely efficient for therapy and diagnostics (theranostics). However, broadband radiation from conventional X-ray sources (such as CT scanners) results in vast and unnecessary radiation exposure. Monochromatic X-ray sources are expected to be considerably more efficient. We have developed a new and comprehensive methodology—*Resonant Nano-Plasma Theranostics* (*RNPT*)—that encompasses the use of monochromatic X-ray sources and high-$Z$ nanoparticles. Ongoing research entails theoretical computations, numerical simulations, and *in vitro* and *in vivo* biomedical experiments. Stemming from basic theoretical studies of K$\alpha$ resonant photoabsorption and fluorescence in all elements of the Periodic Table, we have established a comprehensive multi-disciplinary program involving researchers from physics, chemistry, astronomy, pathology, radiation oncology and radiology. Large-scale calculations necessary for theory and modeling are done at a variety of computational platforms at the Ohio Supercomputer Center. The final goal is the implementation of RNPT for clinical applications.

A.K. Pradhan (✉) · S.N. Nahar
Dept. of Astronomy, The Ohio State University, Columbus, OH 43210, USA
e-mail: pradhan@astronomy.ohio-state.edu

A.K. Pradhan
Biophysics Graduate Program, The Ohio State University, Columbus, OH 43210, USA

A.K. Pradhan
Chemical Physics Program, The Ohio State University, Columbus, OH 43210, USA

M. Mohan (ed.), *New Trends in Atomic and Molecular Physics*,
Springer Series on Atomic, Optical, and Plasma Physics 76,
DOI 10.1007/978-3-642-38167-6_15, © Springer-Verlag Berlin Heidelberg 2013

As an example, we present Monte Carlo numerical simulations for platinum ($Z = 78$) as radiosensitizing agent for killing cancerous cells via increased linear-energy-transfer (LET) and dose enhancement. Radiation therapy in clinical environments is generally administered from high-energy Linear Accelerators (LINAC) emitting broadband 6–15 MeV X-rays with high intensity. Monte Carlo simulations for X-ray energy absorption and dose deposition in tissues were carried out using the Geant4 code for 100 kV, 170 kV and 6 MV broadband X-ray sources. It is found that only X-ray energies ~100 keV are efficient in achieving the required dose enhancement. We confirm previous results for gold ($Z = 79$) that it is the low-energy component around 100 keV from the 6 MV LINAC that is effective in dose-enhanced cell killing. We also describe a simple device for broadband-to-monochromatic (B2M) conversion. A broadband 100 kV source is used to produce monochromatic fluxes in the K-alpha lines from a zirconium ($Z = 40$) target. Monochromatic X-rays such as obtained from B2M conversion should be most effective for theranostics, provided they can be tuned to resonant energies in the targeted material. That is also a quest for X-ray sources such as synchrotrons, high-intensity laser produced plasmas, and accelerator generated free-electron lasers. The project described in this report highlights the fact that interdisciplinary research can be immensely valuable in addressing major problems of heretofore intractable complexity, such as cancer treatment. Approximately 100 news items have appeared on this research in the media; selected links to some articles are given at www.astronomy.ohio-state.edu/~pradhan.

## 15.1 Introduction

Atomic physics provides the link between astronomy and medicine. This review begins with the simplest possible atomic transition 1s–2p. In hydrogen it gives rise to the Lyman-alpha line. In all other atomic systems it is referred to as the K-alpha transition. But in non-hydrogenic atoms and ions there are a large number of K$\alpha$ transitions associated with the 1s–2p transition arrays (for a detailed discussion see [7]).[1] In Sect. 15.2 we describe the most interesting observation of the K-alpha line in astronomy—as spectral signature of black holes. From Sect. 15.3 onwards we discuss in detail the rather unexpected application of the atomic physics of K$\alpha$ transitions in building and using monochromatic X-ray sources for use in biomedical research, and potentially for clinical imaging and therapy. The biomedical physics and methodology is termed *Resonant Nano-Plasma Theranostics* (*RNPT*), *or Resonant Theranostics* (*RT*), and is described in several previous publications [3, 5, 8].

[1] This textbook bridges physics and astronomy and is divided evenly between modern atomic physics and the spectroscopy of astrophysical objects. Figure 15.1b is from the chapter on Active Galactic Nuclei and Quasars. More details are given at the author's webpages: www.astronomy.ohio-state.edu/~pradhan and www.astronomy.ohio-state.edu/~nahar.

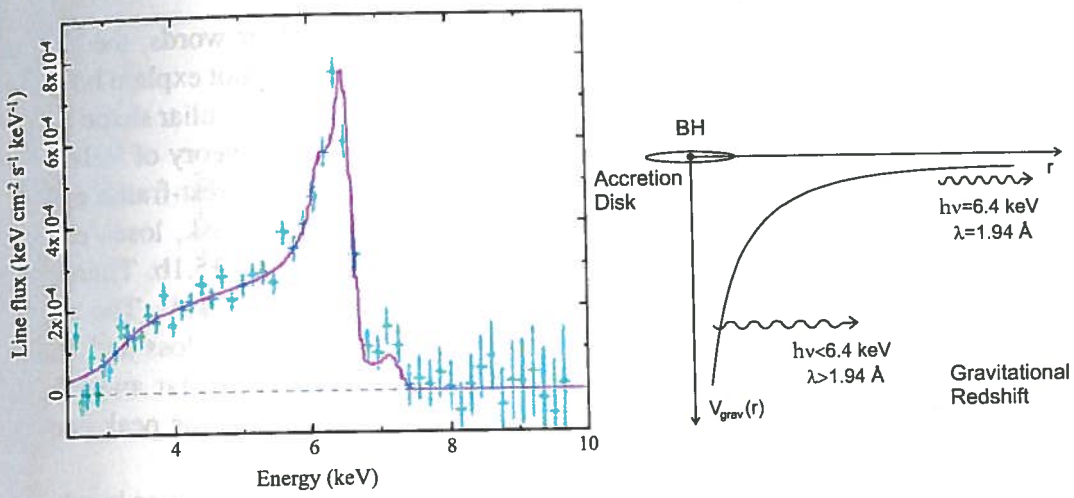


**Fig. 15.1** (**a**) Relativistically broadened Iron K$\alpha$ line first observed by Tanaka et al. [9]. Such asymmetric lines have since been observed from many active galactic nuclei and are regarded as evidence of iron emission in close proximity of supermassive black holes at the center of galaxies. (**b**) Schematic diagram of relativistic broadening and gravitational redshift of photon energy from regions close to the black hole and accretion disk, and farther away (reproduced from Pradhan and Nahar [7], *Atomic Astrophysics and Spectroscopy*, Cambridge University Press, 2011)

## 15.2 X-Rays in Astronomy

How do we know black holes exist? By definition they cannot be seen. Any evidence must necessarily be indirect. Ergo: A preponderance of evidence must be offered before concluding that they exist at all. Indeed, astronomers have by now accumulated a variety of factual observations that lead to that conclusion.

From a physics perspective—even more from the point of view of atomic physics and spectroscopy—the most convincing observation of the existence of a black hole is shown in Fig. 15.1. It is now widely accepted that at the centers of many if not all galaxies must be a supermassive black hole. The reason is that the central regions or nuclei of galaxies exhibit tremendous activity and output of energy at all wavelength ranges of the electromagnetic spectrum, from radio waves produced by relativistic electrons in jets directed perpendicular to the galactic plane, to hard **X-rays** and gamma rays from environments in the vicinity of the black hole and the accretion disk. The energy emitted is so stupendous that no physical process except gravitational infall into the extremely small region inhabited by the black hole can account for the energy budget.

But the most astonishing observation is that of a single atomic line. It is an X-ray line due to the K-alpha 2p $\rightarrow$ 1s transition in iron which corresponds to an energy of 6.4 keV. It arises due to transition(s) between the filled 2p-subshell of iron down to the 1s-subshell, following K-shell ionization by the hard X-rays originating from the immense accretion activity around the black hole. Figure 15.1a shows the line center and profile of this Fe K-alpha line. It is immediately obvious that something is very strange. First of all, the profile is asymmetric. The line center is at 6.4 keV as it should be. But then the profile is extremely broad on the low-energy side; its

"red-ward" broadening extends down to about 4 keV. In other words, the line is broadened by over 3 keV. Plasma or Doppler broadening would not explain both the asymmetry and the width of the line. It is now believed that this peculiar shape is due to gravitational broadening as predicted by Einstein's General Theory of Relativity [9]. A photon emitted in close proximity of the black hole with rest-frame energy of 6.4 keV, from the inner-most stable orbits in the accretion disk, loses energy as it climbs out of the gravitational potential as shown in Fig. 15.1b. Therefore, the photon energy in the observer's frame of reference $E < 6.4$ keV. The closer the emitting iron atom is to the black hole, the bigger the energy loss and larger the broadening. The converse is also true: the Fe K$\alpha$ line emitted far away from the black hole would not experience the gravitational redshift and the peak energy would be at $E = 6.4$ keV.

We note in passing an interesting fact that may not have escaped notice by physicists. The gravitational potential shown in Fig. 15.1b is similar in shape to the coulomb atomic or molecular potential. The $V \sim 1/r$ behavior of both the gravitational and the coulomb potential implies a singularity at the nucleus as $r \to 0$ and $V \to \infty$. And, of course, the gravitational coupling constant is weaker than the electromagnetic coupling constant by a factor of $10^{39}$!

## 15.3 X-Rays in Medicine

But what does this have to do with cancer research? The answer to that question necessitates an in-depth analysis of how X-rays are utilized in medical devices, such as ordinary X-ray machines with Roentgen X-ray tubes and Computerized Tomography (CT) scanners used for 2D and 3D imaging, and linear accelerators (LINAC) used for radiation therapy.

Conventional X-ray sources produce bremsstrahlung broadband radiation over a wide range up to the peak voltage in the X-ray tube. But X-rays at most of these energies are ineffective and result in unnecessary exposure for imaging and therapy. Despite some very low-energy filtration of X-rays with $E \sim 10$–$20$ keV, the remaining low-energy emission does not penetrate to sufficient depths. On the other hand, X-rays with energy more than a few hundred keV are largely Compton-scattered, which is ineffective. High-$Z$ (HZ) radiosensitizing agents are therefore introduced to increase X-ray photoelectric absorption by heavy atoms. Among these agents are platinum compounds and gold nanoparticles [1–4]. Although HZ material embedded in tissue increases dose absorption, the lack of specificity of broadband X-ray sources still results in radiation overdose. It is therefore proposed that monochromatic X-rays would be far more effective, as their energies can be precisely matched to atomic absorption cross sections, and the dosage determined with accuracy a priori.

However, there are two problems. First, a convenient monochromatic X-ray source must be developed. Second, a procedure for efficient photoabsorption of HZ material needs to be implemented. The underlying physical process is inner-shell

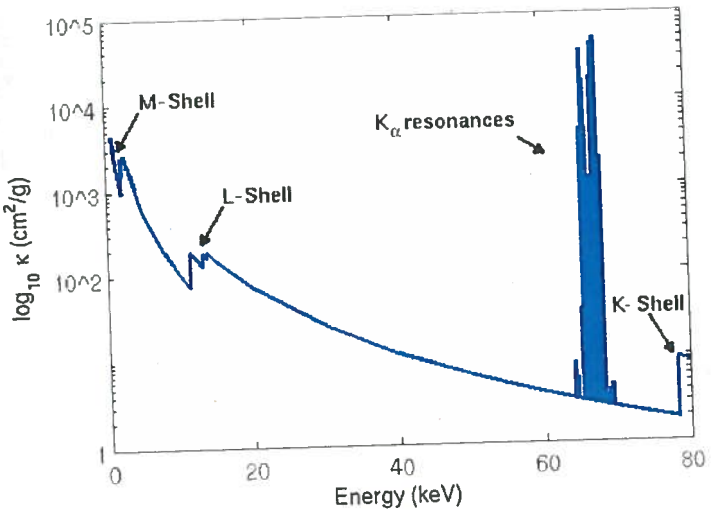


**Fig. 15.2** X-ray attenuation coefficients for platinum as function of incident photon energy. In addition to the M-, L- and K-shell edges we also show the K-alpha resonances superimposed on the smooth background. The Kα resonances may be targeted following K-shell ionization and Auger cascades that result in holes in the upper electronic shells. The region between the Kα and the K-edge is therefore filled with similar resonances that enhance photoelectric absorption by orders of magnitude above the otherwise very low background cross sections [4]

ionization, leading to Auger cascades of secondary electrons. Up to 20 or more Auger electrons may be produced following a single primary K-shell photoionization of HZ elements such as Pt or Au via Coster-Kronig and Super-Coster-Kronig transitions [7]. Most of these electrons have relatively low energies of about 1 keV or less. Therefore their effective impact range is only on nanoscales comparable to the size of the cell nucleus. That localizes the linear-energy-transfer (LET) of Auger electrons resulting in cell killing without damage to surrounding cells.

While HZ compounds or nanoparticles may act as contrast agents, they cannot be effective for X-ray energies much higher than 100 keV. The reason is that after the K-shell jump, the photoabsorption cross sections decrease rapidly with energy. For example, Fig. 15.2 shows X-ray attenuation coefficients due to photoelectric absorption by platinum (Pt). The K-shell energies for the generally safe heavy elements are well below 100 keV; for example they are 81 keV and 78 keV for Au and Pt respectively. However, high-energy Linacs generating X-rays up to 6 to 18 MeV are commonly used for radiation therapy. It follows that for dose enhancement using HZ radiosensitizers only the relatively low-energy component around 100–200 keV from the high-energy Linacs is likely to be effective. Similar to earlier work on Au nanoparticles [1, 2, 4, 8], we verify this hypothesis in the present study.

Another serious problem in conventional theranostics is the use of broadband radiation that lacks specificity in its interaction with HZ material. Figure 15.1 shows the existence of features in the attenuation coefficients or cross sections for photoabsorption of X-rays by Pt. It is clear that these features can be targeted using monochromatic X-rays at resonant frequencies. In earlier works [3, 5] we have shown that monochromatic irradiation at resonant energies will allow the creation of inner-shell vacancies. In principle it is then possible to not only ionize the K-shell

electrons that result in corresponding holes in all electronic shells, but also excite the K$\alpha$ resonances. This combination of resonant K-shell ionization-excitation would *accelerate* the induced Auger effect and corresponding X-ray energy deposition. Numerical simulations for Au atoms show that HZ radiosensitization using X-rays tuned to these resonances can cause an 11-fold increase in the dose absorbed by the tumor [3].

Considerable work has also been carried out using Au nanoparticles in experiments and models [9]. Simulations demonstrate that X-ray irradiation at about 100–200 keV has the highest dose enhancement factors (DEF) and is most effective in cell killing. In this study we examine the sensitivity due to Pt, which is commonly used in chemotherapy as cisPt, carboPt, and other compounds.

## 15.4 Resonant Enhancement of Auger Effect

In order to understand in more detail the basis for therapy based on radiosensitization of HZ atoms, it is necessary to examine the Auger process and the pathways in which it manifests itself upon irradiation by incident X-ray X-rays. The atomic structure and radiative and autoionization processes play the dominant role. Figure 15.3 illustrates the Auger processes-ejection of electron(s) upon ionization of an inner shell by X-ray photon(s).

Figure 15.3a shows the Auger effect: a transition K $\rightarrow$ L followed by a radiationless ejection of an electron from an outer shell. Special cases are: Coster-Kronig transitions, when a transition within the L-shell results in ejection of en electron from another shell (M), and Super-Coster-Kronig transitions where both the initial transition and the ejected electron are from the same shell (N).

Figure 15.3b is a diagram that highlights two main features underlying the RNPT mechanism. First, an X-ray photoionization from the K-shell can lead to multiple electron vacancies in the outer shell; the number of holes can double in each outer shell, as shown. Second, the Auger cascades may be reversed by resonant irradiation by photons exactly equal in energy to the transitions K$\alpha$, K$\beta$, etc. Employing high-intensity monochromatic X-ray sources, such resonant absorption, and hence enhancement of the "Auger cycle" may be implemented. However, it is clear that a monochromatic and precisely tuned X-ray source is required.

## 15.5 Resonant Nano-Plasma Theranostics (RNPT) Methodology

A basic sketch of an experimental scheme to implement RNPT [3, 5, 8] is shown in Fig. 15.4. A monochromatic X-ray source and suitable HZ material can be combined for both imaging and therapy. The former depends on fluorescence from the atoms undergoing Auger decays. The latter is the outcome of resonantly enhanced absorption that would release Auger electrons capable of killing adjacent cells.

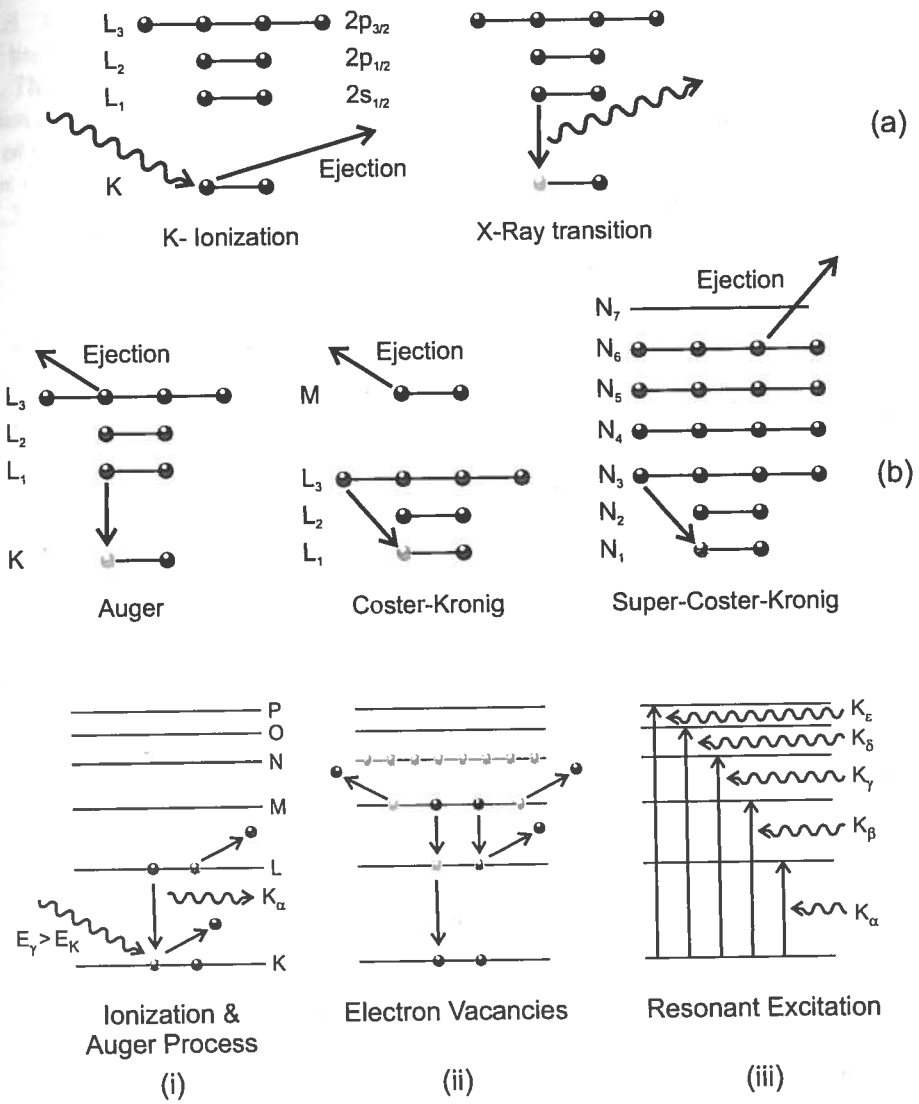


**Fig. 15.3** (**a**) The Auger process and Coster-Kronig and Super-Coster-Kronig transitions (Pradhan and Nahar [7], Chap. 5, *Atomic Astrophysics and Spectroscopy*, Cambridge University Press, 2011) (**b**) (*i*) K-shell ionization followed by Auger decays, (*ii*) multiple electron vacancies propagate to outer shells, (*iii*) resonant excitation by K$\alpha$, K$\beta$, etc. Resonance fluorescence induced by monochromatic X-ray beams can enhance Auger decays, resulting in localized energy deposition and Auger electron-photon emission in high-$Z$ atoms (nanoparticles) that capable of killing cancerous cells [3, 5, 8]

The **RNPT** methodology also requires a significant development in nanobiotechology: design, targeting, and delivery of nano-moieties to the cancerous cells. Considerable progress in being made in both areas, the development of high-intensity monochromatic sources, as well as HZ nanoparticles, particularly gold nanoparticles that are safe and sufficiently heavy for optimal radiosensitization. Among the X-ray sources being explored are high-powered laser produced plasmas, free-electron lasers, and synchrotrons.

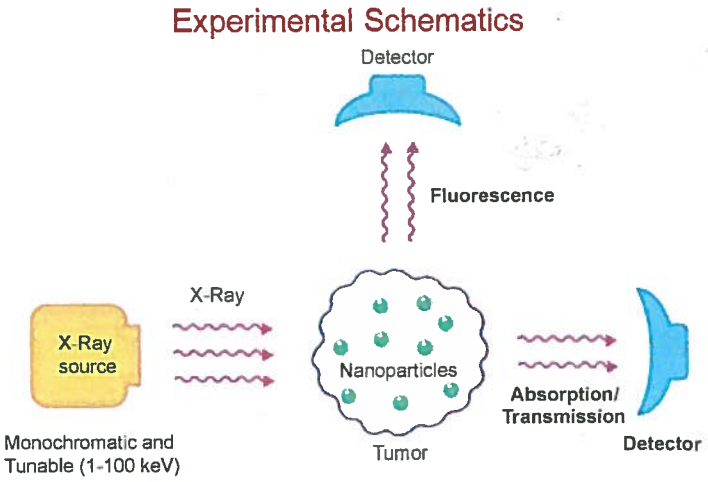


**Fig. 15.4** Schematic diagram for implementation of the RNPT methodology for theranostics. The detector on top perpendicular to the monochromatic beam is for imaging via fluorescence from the high-$Z$ nanoparticles embedded in the tumor. The detector along the same direction as the X-ray beam measures the radiation dose absorbed and delivered to the tumor

## 15.6 Radiosensitization Using Broadband X-Ray Sources

In this section we describe computational work using existing X-ray machines producing broadband radiation but in very different energy ranges. We consider three broadband X-ray sources in our numerical simulations: 100 kV, 170 kV and 6 MV. Their output spectra are shown in Fig. 15.5 for the former two devices and in Fig. 15.6 for a 6 MV Linac. In Fig. 15.5 the K-alpha energy and the K-shell ionization energy of Pt are marked. Each K-shell ionization in a HZ atom generally results in K$\alpha$ emission, triggering Auger electron cascades that create vacancies in upper L, M, N, O and P electronic shells of the **platinum** atom. Therefore, it is possible to resonantly excite electrons from the K-shell into higher shells. The large resonant coefficients for K$\alpha$ excitation are shown in Fig. 15.2. The Resonant Nano-Plasma Theranostics (RNPT) methodology has been proposed to implement the Auger trigger and *in situ* enhancement of localized X-ray energy deposition via resonant excitation using monochromatic X-rays [5, 8].

**Dose Enhancement:** Dose enhancement factor (DEF) is defined as the ratio of radiation dose absorbed with and without a radiosensitizing agent. In general the simulations and calculations of DEFs are quite involved. One needs a realistic model of the targeted and intervening tissue in the body. The usual approach is to assume a configuration called a "phantom". The tissue at each depth along the phantom and the interaction of X-ray radiation must then be computed at various depths as it traverses the body. Concentration of HZ moieties embedded in the targeted tissue must also be taken into account. Such simulations require a sophisticated computational program. We employed a general-purpose open software package for Monte Carlo simulations Geant4, as described in the next section.

**Numerical Simulations:** We adapted the Geant4 toolkit version 9.4 to simulate the deposition of X-ray energy through human tissue with the use of a 15 cm × 5 cm × 5 cm water phantom. A tumor was simulated using a 2 cm × 5 cm × 5 cm region located 10 cm into the phantom. This region was filled with a 7.0 mg/ml concentration of Pt homogeneously distributed in water to simulate the presence of Pt radiosensitizers in tumors.

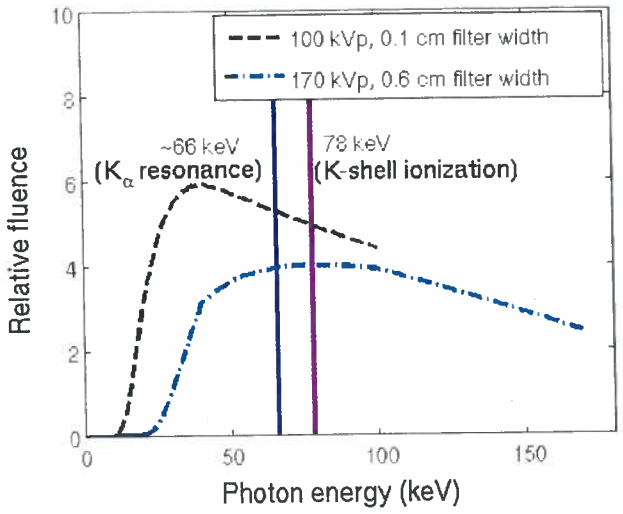


**Fig. 15.5** The 100 kV and 170 kV bremsstrahlung spectra. The K-shell ionization energy and average energy of the Kα resonance complex of Pt shown in Fig. 15.2 are marked

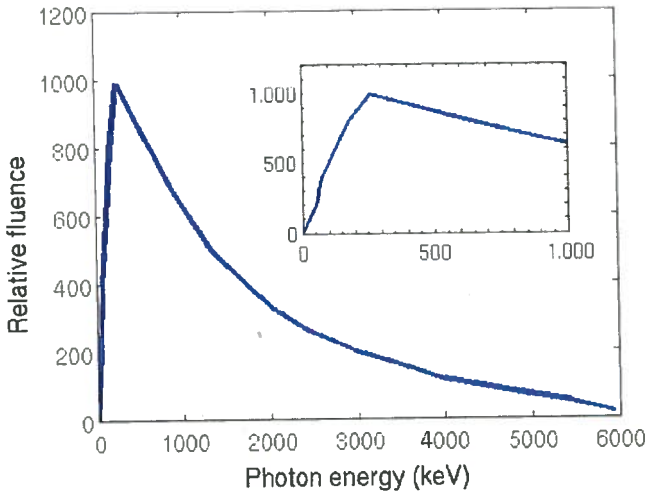


**Fig. 15.6** The 6 MV LINAC bremsstrahlung spectrum. The peak around 200 keV results from filtering the lower energy X-rays

The physical interactions of Pt and water with X-rays were governed by the atomic data built into Geant4. These atomic coefficients also determine the background photoabsorption by Pt as in Fig. 15.2. Photon fluence for each broadband source was determined using the spectra shown in Figs. 15.5 and 15.6. Energy intervals of 10 keV at low energies (<500 keV) and 500 keV for higher energies were used.

We calculated DEFs for radiation therapy using a 6 MV Linac, compared to the relatively low energy range from the 100 kV and 170 kV. At each energy interval, the **X-rays** were tracked as they traveled through the phantom, with the total dose absorbed by the tumor model recorded. No difference in dose enhancement was seen with the tumor region located near the surface of the phantom compared to deep inside it. **Dose** deposition was determined for the tumor phantom containing either 7.0 mg/g or 0 mg/g, representing a tumor with and without radiosensitizers respectively. Dose enhancement due to Pt was then determined by dividing the dose in tumor with Pt over the dose delivered to the tumor without Pt.

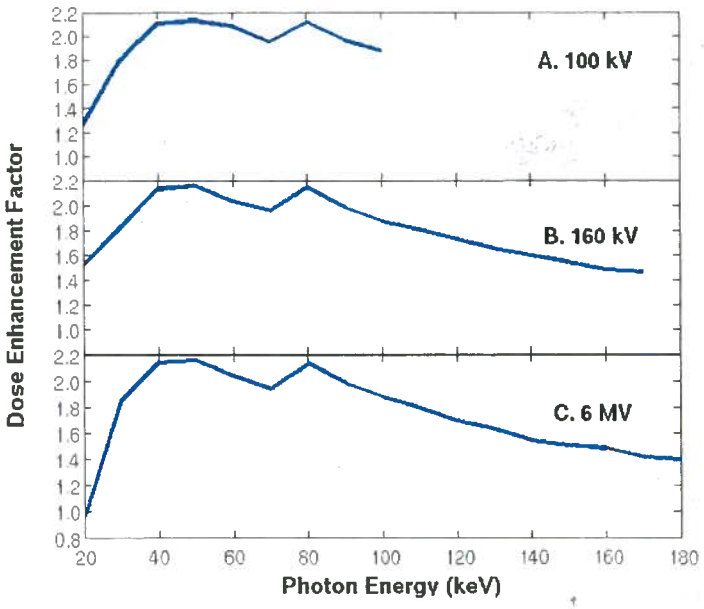


**Fig. 15.7** Similarities in dose enhancement factors with platinum radiosensitization and X-ray irradiation from different broadband sources: **A**. 100 kV, **B**. 170 kV, **C**. 6 MV [3]

Figure 15.7 shows the dose enhancements achieved using a 100 kV, 170 kV and 6 MV photon sources. As can be seen, dose enhancements peak at low energies ($E < 100$ keV). The explanation for the double-peaked structure is as follows. The low energy X-rays in the otherwise bremsstrahlung spectrum are assumed to be filtered out. The combination of low-energy filter and L-shell ionization produces the first peak around 40 keV. The DEF decreases thereafter until the second peak at approximately 80 keV corresponding to the K-shell ionization of Pt (Fig. 15.1). Dose enhancements decrease monotonically after K-shell ionization since there are no other absorption features in Pt photoabsorption cross section that induce another rise in the DEF. The interesting point however is that the DEF tends to a constant value at energies above 250 keV. At this and higher energies, Compton scattering predominates instead of photoelectric absorption [4]. Since there is little difference in attenuation due to largely elastic Compton scattering for both water and Pt, DEF's are small in the high-energy range $E > 250$ keV.

These results lead to two conclusions: first, dose enhancement characteristics of HZ radiosensitizers are largely due to photoionization and subsequent Auger ejections of electrons. That causes the enhancement in the DEFs shown in Fig. 15.7. The second is that elastic scattering dominates photoelectric absorption from about 200 keV onwards, and is relatively constant up to all higher energies even into the MeV range characteristic of Linacs. Therefore no further enhancement of DEF is possible. Also, these high-energy X-rays deposit very limited amounts of their energy to the tumor—the attenuation coefficients of HZ radiosensitizers at these energies are only slightly above that of normal tissue.

Figure 15.8 illustrates these two points and the low and high energy behavior of the Pt DEF using a 6 MV Linac. Following the peak around 200 keV the DEF falls rapidly to a constant value with very little enhancement up to the maximum energy 6 MeV. The drop thereafter is due to negligible interaction of X-rays with atomic species and the final limiting value of DEF is unity.

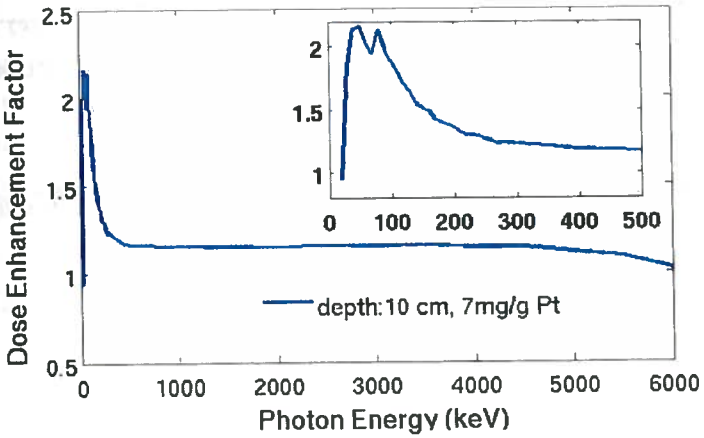


**Fig. 15.8** Dose enhancement factors with a 6 MV source and Pt reagent. The DEF peaks at approximately 100 keV and then drops to low and relatively constant values up to high MeV energies. It is evident that there is little dose enhancement due to radiosensitization at energies higher than 100–200 keV, and that LINACs with MeV X-ray output are not effective throughout most of the energy range

**Experimental X-Ray Irradiation:** The numerical simulations presented herein will be tested experimentally. The experiments are in progress in several stages. First, specific cancer cell lines, such as F98 rat glioma (brain cancer) cells, are prepared. Second, they are treated with Pt compounds such as platinated dendrimers, cisPt or carboPt. Third, the radiosensitized cell lines are then irradiated using 168 kV and 6 MV sources. Fourth, measurements of the cell survival fractions are made to validate the models. The aim is to verify the proposition that it is the low energy component of the broadband spectrum that results in effective cell killing; the high energy component has little effect on the DEF and survival fractions.

## 15.7 Broadband-to-Monochromatic Conversion

Experimental results from a broadband-to-monochromatic (B2M) device are given, as well as modeling results from Geant4 simulations of DEFs using various broadband devices. We first report proof-of-principle results from a device to convert broadband radiation from a conventional X-ray source into largely monochromatic radiation at the K$\alpha$, K$\beta$ energies [3]. This is achieved via fluorescent emission resulting from K-shell ionization of an element (Fig. 15.3a). For example, Fig. 15.9 shows experimental results using an ordinary 100 kV simulator and a zirconium target. The input spectrum is as in Fig. 15.3. The output spectrum in the top panel of Fig. 15.4 shows the Zr K$\alpha$ lines above the scattered background; the isolated features after subtracting the background are shown in the bottom panel.

Using different HZ targets, it is possible to obtain monochromatic flux via K$\alpha$ fluorescence at higher energies that would enable greater penetration in the human body. Figure 15.9 demonstrates that conversion of **X-rays** from a broadband

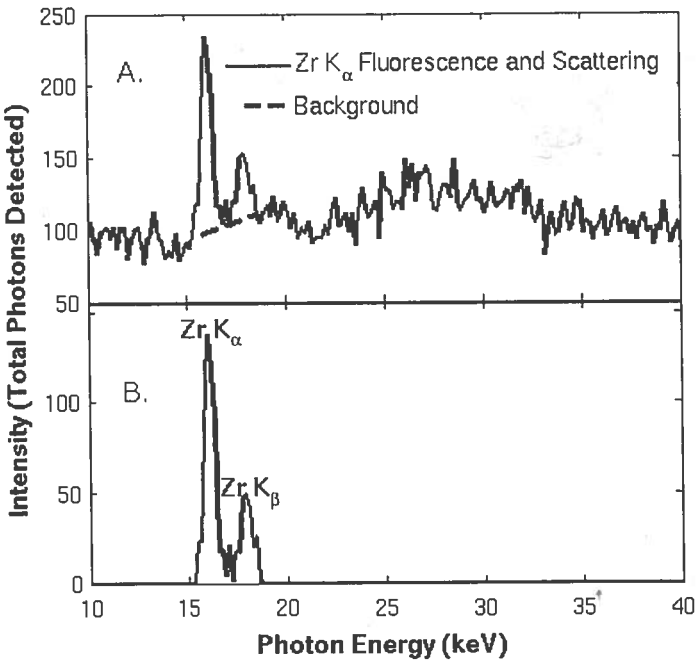


**Fig. 15.9** Monochromatic Kα line fluxes detected after conversion of the bremsstrahlung output from a 100 kV broadband X-ray machine [3]. The *top panel* shows the monochromatic flux together with the Compton scattered background; the *bottom panel* shows the isolated features

source to largely monochromatic spectrum is feasible. Moreover, Kα fluxes can be produced at a range of desired energies by selecting different HZ targets. However, the intensity is still insufficient to enable imaging and therapy to the extent needed for clinical applications and more experimental work is required. The B2M conversion efficiency is estimated to be around 0.02. Much lower monochromatic flux is required to activate the targeted features in photoabsorption (Fig. 15.2) than from broadband sources such as simulated in this report. The resulting **DEFs** from monochromatic X-ray irradiation should be considerably higher than obtained herein (Fig. 15.7).

## 15.8 Conclusion

We conclude this review by highlighting the main features.

1. Based on atomic and astrophysical X-ray spectroscopy, a new methodology—Resonant Nano-Plasma Theranostics (RNPT) has been developed [3, 5, 8]. It aims to complement or supplant existing X-ray devices used for radiation therapy by utilizing monochromatic X-ray sources and high-$Z$ nanomaterials.
2. Heavy elements such as Pt or Au, and HZ compounds, are subject to Auger decays of secondary electrons upon X-ray irradiation which can efficiently kill malignant cells with minimal collateral damage.
3. A general pattern is demonstrated in the behavior of the DEF with a peak of ~2.2 close to the L- and K-edges of HZ material. The low energy range $E < 100$ keV is most effective, and drops substantially to a constant value of ~1.2 for $E >$ 250 keV.

4. The results confirm earlier studies using Au nanoparticles [4]. These studies on both Au and Pt should be of considerable interest to the biomedical community pertaining to the use of high-energy megavoltage radiation up to 6–10 MV in conjunction with HZ radiosensitization.
5. Monochromatic X-ray sources would be most efficient for imaging and therapy since they can be tuned resonantly to specific features that enhance photoabsorption, thereby enabling contrast and radiosensitization with minimum of radiation exposure. While we have presented first results from a proof-of-principle device for B2M conversion, more experimental work is needed to generate required monochromatic fluxes.

**Acknowledgements** We would like to thank our close collaborators from several disciplines on the myriad developments underlying the RNPT mechanism. In particular we would like to acknowledge Yan Yu and his medical physics team in the department of Radiation Oncology at the Thomas Jefferson University Medical School in Philadelphia, Pennsylvania. Max Montenegro and Sara Lim have carried the Geant4 simulations reported herein. Biomedical experimental research at the Ohio State University is primarily due to Rolf Barth (Pathology), Erica Bell (Radiation Oncology), Enam Chowdhury (Physics), Russell Pitzer (Chemistry) and Claudia Turro (Chemistry).

## References

1. R.I. Berbeco, W. Ngwa, G.M. Makrigiorgos, Localized dose enhancement to tumor blood vessel endothelial cells via megavoltage X-rays and targeted gold nanoparticles: New potential for external beam radiotherapy. Int. J. Radiat. Oncol. Biol. Phys. **1**(81), 270–276 (2011)
2. S. Jain, J.A. Coulter et al., Cell-specific radiosensitization by gold nanoparticles at megavoltage radiation energies. Int. J. Radiat. Oncol. Biol. Phys. **79**(2), 531–539 (2011)
3. S. Lim, M. Montenegro, A.K. Pradhan, S.N. Nahar, E. Chowdhury, Y. Yu, Broadband and monochromatic X-ray irradiation of platinum: Mone Carlo simulations for dose enhancement factors and resonant theranostics, in *Proceedings of the 2012 World Congress on Medical Physics and Biomedical Engineering*, Beijing, May (2012), pp. 26–31
4. M.K.K. Lueng, J.C.L. Chow et al., Irradiation of gold nanoparticles by X-rays: Monte Carlo simulation of dose enhancements and the spatial properties of the secondary electrons production. Med. Phys. **38**, 624–631 (2011)
5. M. Montenegro, S.N. Nahar et al., Monte Carlo simulations and atomic calculations for Auger processes in biomedical nanotheranostics. J. Phys. Chem. A **113**(45), 12364–12369 (2009)
6. S.N. Nahar, A.K. Pradhan, S. Lim, K-$\alpha$ transition probabilities for platinum and uranium ions for possible X-ray biomedical applications. Can. J. Phys. **89**, 483–494 (2011)
7. A.K. Pradhan, S.N. Nahar, *Atomic Astrophysics and Spectroscopy* (Cambridge University Presss, Cambridge, 2011)
8. A.K. Pradhan, S.N. Nahar et al., Resonant X-ray enhancement of the Auger effect in high-$Z$ atoms, molecules, and nanoparticles: potential biomedical applications. J. Phys. Chem. A **113**(45), 12356–12363 (2009)
9. Y. Tanaka et al., Gravitationally redshifted emission implying an accretion disc and massive black hole in the active galaxy MCG-6-30-15. Nature **375**, 659 (1995)